Beamtest of Non-irradiated and Irradiated ATLAS SCT Microstrip Modules at KEK

Y. Unno[1], T. Matuo[2], T. Hashizaki[2], T. Akimoto[8], J. Bernabeu[10], Z. Dolezal[4], L. Eklund[9], K. Hara[8], Y. Ikegami[1], Y. Iwata[5], Y. Kato[8], C. Ketterer[3], H. Kobayashi[8], T. Kohriki[1], T. Kondo[1], T. Koshino[2], J. Ludwig[3], T. Masuda[5], G. Moorhead[7], I. Nakano[2], K. Norimatsu[2], T. Ohsugi[5], K. Runge[3], S. Shinma[8], R. Takashima[6], R. Tanaka[2], N. Tanimoto[2], S. Terada[1], N. Ujiie[1], M. Vos[10], K. Yamanaka[5], and T. Yamashita[2]

[1]Institute of Particle and Nuclear Studies, High Energy Accelerator Research Organiation (KEK), Tsukuba 305-0801, Japan
[2]Physics department, Okayama University, Okayama 700-8530, Japan
[3]Department of Physics, Albert-Ludwig University of Freiburg, D-79104 Freiburg, Germany
[4]Institute of Particle and Nuclear Physics, Charles University, CZ-180 00 Prague 8, Czech Republic
[5]Physics department, Hiroshima University, Higashi-Hiroshima 739-8526, Japan
[6]Education department, Kyoto University of Education, Kyoto 612-0863, Japan
[7]School of Physics, University of Melbourne, Parkville, Victoria 3052, Australia
[8]Institute of Physics, University of Tsukuba, Tukuba 305-8571, Japan
[9]Department of Radiation Science, Uppsala University, S-75121 Uppsala, Sweden
[10]Institute Fisica Corpuscular, Universidad de Valencia, E-46017 Valencia, Spain

Abstract

Non-irradiated and irradiated ATLAS SCT barrel and forward modules were beamtested with 4 GeV/c pions. Pulse shapes confirmed the peaking time of the amplifier to be 22 ns and deteriorated slightly in the irradiated modules. Median charges saturated around 3.8 fC both in the non-irradiated and irradiated modules. Signal/Noise ratios, using the noises from the in-situ calibration, were >16 in the non-irradiated (>150 V), and >10 in the irradiated (>300 V) barrel modules. No excess common-mode noise was observed.

I. Introduction

Two beamtests [1] were carried out at KEK using pion beams of 4 GeV/c at its 12 GeV proton synchrotron, for measuring the performance of the fully equipped SCT modules in an environment of experiment. These were the first beamtests of the SCT modules, succeeding the beamtests of components [2]. Since the results of the second beamtest covered the results of the first test, only those of the second test were presented in this paper.

II. SCT silicon microstrip modules

A. ATLAS SCT silicon microstrip sensor

After intensive studies of the radiation damage and developments of radiation-tolerant designs, ATLAS SCT has chosen a type of silicon microstrip sensors of p-implant strips in the n-bulk silicon wafers, so-called p-in-n sensors. One type of sensor, square, is used for the barrel modules and 5 types of wedge sensors for the forward-backward (abbreviated as “forward”) modules. The sensors are designed to have a mean strip pitch of 80 µm at the centre of a module.

B. Frontend readout ASIC

The signals from the strips are read out with a frontend electronics with high gain (50mV/fC), unipolar fast shaping (20 ns peaking time), on-off discriminating (binary), and buffering the digitized bits for 3.3 µs duration. The SCT specific design, named ABCD, is implemented in a BiCMOS single chip application-specific-integrated-circuit (ASIC) in a radiation-tolerant technology [3]. One ASIC is made of 128 channels.

C. Barrel and forward modules

The SCT modules are designed to have a strip length of 12 cm and two coordinate sensing in a module. A pair of sensors are glued on the top and the bottom of a baseboard at an angle of 40 mrad. A module is equipped with 12 ABCD chips on a hybrid, 6 on the top and 6 on the bottom side. The hybrid is placed near the centre of the module in the barrel modules, wrapping around, and at the end in the forward modules, double-sided. The designs are driven principally by the difference in cylindrical and disk geometries. Photographs of the barrel and forward modules are shown in Figure 1 and Figure 2.

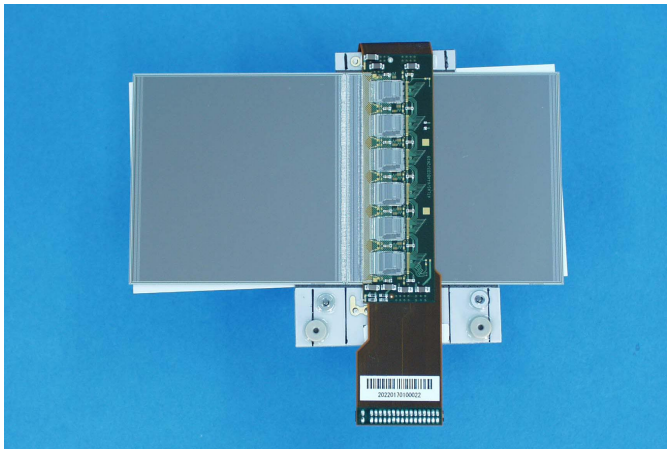

Figure 1: ATLAS SCT barrel module

Two modules, one barrel and one forward, were irradiated prior to the beamtest to the fluence of 3×10^{14} protons/cm^2 at the 24 GeV proton synchrotron at CERN, equivalent to the 2×10^{14} 1 MeV neutrons/cm^2.

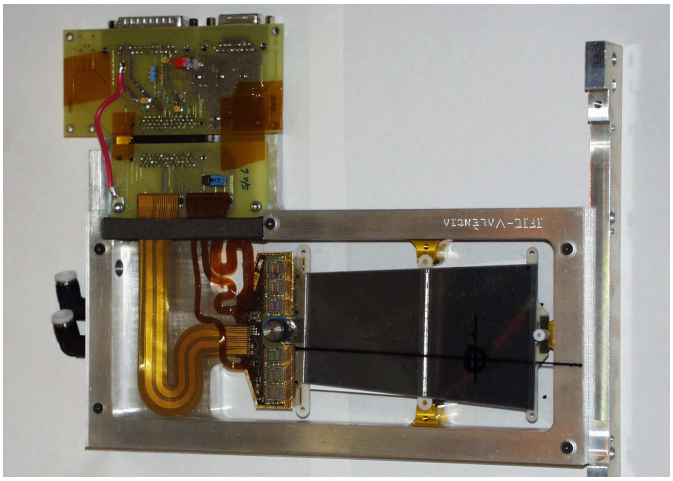

Figure 2: ATLAS SCT forward modules, together with a module frame and a readout card of the beamtest

III. BEAMTEST

A. Setup

Two beamtests were carried out. Two barrel and one forward modules with ABCD2T chips were tested in the first, and three barrel and three forward modules with ABCD3T chips, including two irrradited modules, were tested in the second beamtest. A classification of the modules is summarized in Table 1 [4].

Table 1
Name, type, ASIC, and irradiation characteristics of the modules in two beamtests

Beamtest		Name	Type	ASIC	Irradiation
1		k3103	barrel	ABCD2T	non-irrad
		FR-k81	forward	ABCD2T	non-irrad
		k3104	barrel	ABCD2T	non-irrad
2	mod1	011	barrel	ABCD3T	non-irrad
	mod2	022	barrel	ABCD3T	non-irrad
	mod3	003	barrel	ABCD3T	irrad
	mod4	VAL-k3-166	forward	ABCD3T	irrad
	mod5	VAL-k3-165	forward	ABCD3T	non-irrad
	mod6	CG-k3-170	forward	ABCD3T	non-irrad

The modules were attached to aluminium module frames and positioned in a thermo-box in the beamline. Three “Si-telescopes” were placed, in sandwiching two modules in between, in order to provide a position resolution of about 5 µm in horizontal and in vertical directions. The modules were separated by 30 mm each other. The smearing by multiple scattering was estimated to be negligible by interpolating the positions of the incident particles with two adjacent telescopes. The incident particles were triggered with the scintillators of 2 cm x 2 cm placed in the upstream.

The modules were cooled in two ways: the overall environment inside the thermo-box was cooled with a circulation of cold air of about -20 °C, and, in addition, the irradiated modules were cooled with a liquid cooling of about -13 °C. The temperatures of the barrel hybrid were about 0 °C.

B. Trim range setting in the irradiated modules

After the irradiation, ABCD3T chips showed a problem in setting the trim DAC range of the trim circuitry. (This problem was fixed in the latest ABCD3TA chips.) The ranges were stuck to 1 and 2 in mod3 and 2 and 3 in mod4, in the 4 chips where the beam particles passed (beam spot). The resulting masked channels which were out-of-trimming were, however, small: 1 and 4 channels in the mod3 and the mod4 modules, respectively.

C. Charge calibration

The relations of the threshold voltages and the charges were calibrated, in situ, by injecting charges with the internal circuitry in the ABCD chips. The internal calibration circuitry required several correction factors: deviation of the capacitance values of the charge injection capacitors, deviation of charge scales due to the chip temperatures and radiation damages. These factors were measured and/or estimated as in Table 2. The charge scales were multiplied by the Total factors.

Table 2
Charge correction factors due to calibration capacitance (Cap), temperature (Temp), irradiation(Irrad), and combined total(Total)

mod	Name	Cap	Temp	Irrad	Total
1	011	1.07	1	1	1.07
2	022	1.07	1	1	1.07
3	003	1.07	1	0.97	1.04
4	166	1.07	0.95	0.97	0.99
5	165	1.07	0.97	1	1.04
6	170	1.07	0.97	1	1.04

D. Data taking and analysis

Data were taken by varying two parameters: the sensor bias voltage between 25 and 275 V for the non-irradiated and 150 and 500 V for the irradiated modules, and the threshold between 0.7 and 6 fC. In the following analyses, the conditions taken for a typical setting were, otherwise mentioned, (1) bias voltages of 150 V and 350 V for the non-irradiated and the irradiated modules, and (2) threshold at 1 fC. In the plots, the voltages of the irradiated modules were corrected for the voltage drops in the series resistance in the bias supply lines.

IV. DATA ANALYSIS

A. Pulse shape reconstruction

The ABCD chip has a discriminator circuitry with two modes. One of them is a sampling at the phase of the clock. With an externally supplied self-running clock, the signal pulses, after the amplification and shaping, are sampled continuously since the arrival time of particles and the clock phase is random. Combining the threshold scanning and the measurement of the time between the triggers and the clock phase, the time distribution of the median pulse heights can be reconstructed.

The ABCD chips were clocked at 40 MHz and the time between the triggers and the clock phase were measured with a TDC in the beamtest. The resulting time distributions of the median pulse heights are shown for the non-irradiated (average of mod1 and mod2) and for the irradiated (mod3) modules in Figure 3. The positions of the peaking were adjusted to be at 40 ns. The impulse response curves of a first-order differential and third-order integration circuitry, CR-RC^3, were fitted in the rising part of the pulses, between 20 and 45 ns. The peaking time of the non-irradiated module was 22 ns and that of the irradiated one was 27 ns. The peaking time of the non-irradiated chips was consistent with the ABCD specification. The peaking time of the irradiated module was slower due to a slower charge collection in the radiation-damaged sensors and a slower speed of the damaged amplifiers.

Other distinctive feature of the reconstructed pulses was the shoulders seen after the peaking. This shoulder could not be reproduced in the simulation of the charge collection in the damaged sensors. Since the shoulder was said not observed in the chips without the discriminators [5], this would be a physical feedback of the discriminator shocks. Compared to the barrel modules, larger excess shoulders were observed in the forward modules.

In the following analyses, an event selection was applied to those events which time was in the peak region, between 35 and 45 ns. No correction was made to the range in other bias voltages since the move of the peak position was small.

B. Position resolutions

In a sensing plane of a module, consecutive hit-strips were clusterized to define a hit-cluster, with the geometrical centre as the position of the "cluster centre" and the number of strips as the "cluster width". The trajectories of the incident particles were made with two adjacent telescopes in order to minimize the effect of multiple scattering. The deviations of the cluster centres from the trajectories were the position resolution of the sensing plane.

The deviation distributions of the module, mod1, is shown in Figure 4, for all events (circle) and for the cluster width greater than 1, the "multi-hits", (diamond). The distribution of all events is close to the uniform distribution of the pitch, 80 μm. That of the multi-hits is much narrower due to the fact that the multi-hits occurs where the particles hit in the midway between

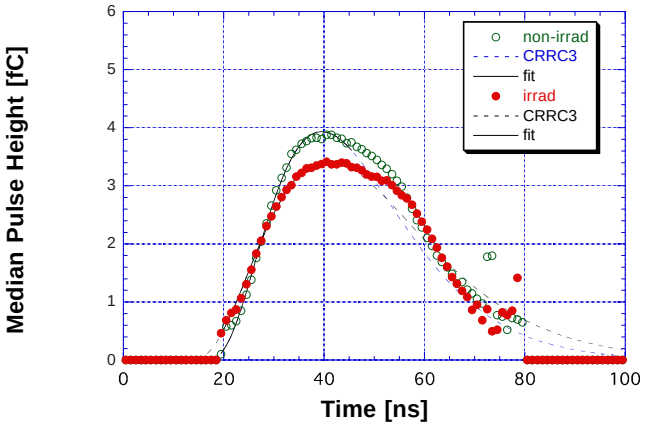

Figure 3: Median pulse height distributions as a function of time to the triggers: non-irradiated (open circle) and irradiated (filled circle) modules, and the impulse responses of CR-RC^3 circuitry (solid line being the fitted region) with the peaking times of 22 and 27 ns, respectively

the strips, effectively reducing the width of the sensitive region.

In order to derive the root-mean-square (RMS) resolution of the uniform distribution, the Gaussian functions were fitted, without weighting, and the Gaussian sigma was reduced by a factor 1.24 associated to the difference in the RMS and the Gaussian standard deviations when fitted to the uniform distribution. The resulting RMS resolutions were 22.5 μm and 10 μm for the all and multi-hits events, respectively.

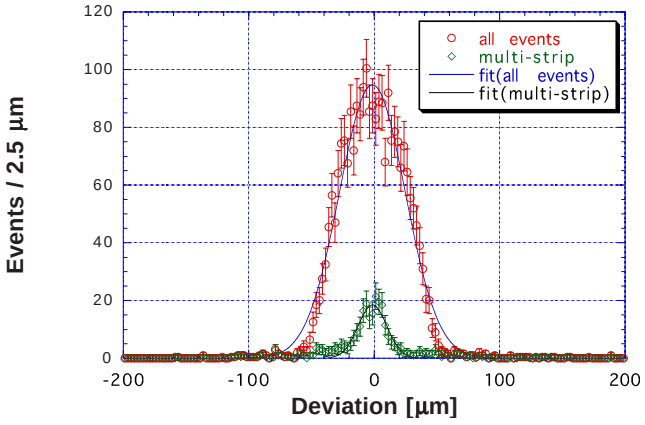

Figure 4: Deviations of the cluster centre from the expected positions of incident particles of the mod1 module: all events (circles) and the events with multi-hits (diamonds), with Gaussian fits, without weighting

In analysing the forward modules, a correction to the fan geometry was taken into account to project the hit at t=(x, y) to the x axis defined at a pitch, p, approximated as

$$xp = x + ((d\theta)/(dx)) \cdot x \cdot y\,. \qquad (1)$$

The pitch evaluated was 86 μm where the beam spot was.

The RMS resolutions of the barrel and the forward modules were about 23 µm and 26 µm, consistent with the pitch of 80 µm and 86 µm, respectively, although those of the forward modules were slightly worse than the expected.

C. Efficiency scans and Median charges

Counting the hits with the cluster centres within a window of the incident particles (full width of 500 µm in the analysis), an efficiency at a threshold can be obtained. Although the electronics is one threshold, the pulse height (Landau) distribution is reconstructed as an efficiency curve by scanning the threshold. Such an example is shown in Figure 5 for the irradiated module, mod3, together with the scanning of bias voltage. The threshold of the 50% efficiency is the median charge of the pulse height (Landau) distribution.

In order to obtain the threshold of 50% efficiency, a modified error function, eq. (2), was fitted to the efficiency scans,

$$eff(q) = p_3(1 - erf(T \cdot f(T))) \quad (2)$$

where

$$f(T) = 1 + 0.6 \cdot tanh(-p_4 \cdot T) \text{ and} \quad (3)$$

$$T = (q - p_1)/(\sqrt{2} \cdot p_2)\,. \quad (4)$$

The function, erf, was the integral of the Gaussian distribution. The function, $f(T)$, is an empirical function to modify the Gaussian to the Gaussian-convoluted Landau distribution. The fitting parameters expressed the median (p_1), the width (p_2), the saturation (p_3), and the skew (p_4).

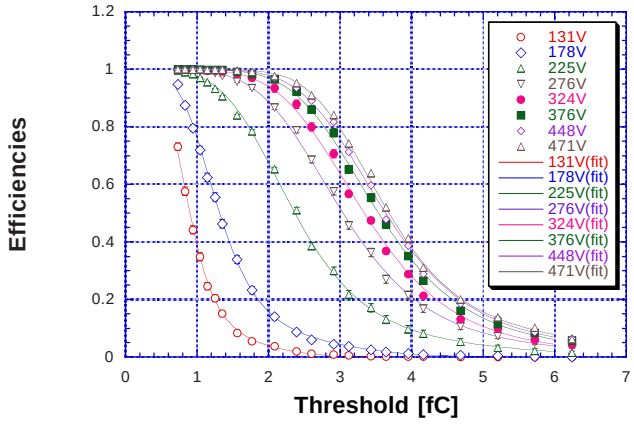

Figure 5: Threshold scan of the efficiencies at various bias voltages in the irradiated barrel module, mod3. The lines are fits to the empirical formula in the text

The median charges of the modules obtained were shown as a function of the bias voltage in Figure 6. The median charges of the non-irradiated modules were saturating above 150V to the charges between 3.8 fC and 4.0 fC. The saturations of the median charges of the irradiated modules were slower and reaching around 3.8 fC at 500V. The full depletion voltages of the non-irradiated and irradiated sensors were about 70 V and

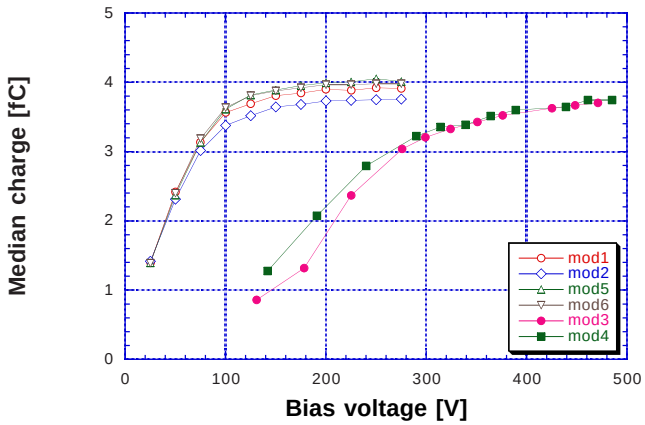

Figure 6: Bias voltage dependence of the median charges.

300 V, respectively.

The median charges of the two non-irradiated barrel modules were not coinciding, nor those of the barrel and the forward modules. These differences would be attributed to the chip-by-chip variation of the calibration capacitance and insufficient corrections on calibration scales due to temperature and radiation damages.

D. Noise occupancies and ENC

Noise hits due to the electronics noises were counted which were out of time (time < 16 ns) and out of track window (2*efficinecy window). The resulting number of hit strips were divided by the number of strips outside the track window, obtaining the noise occupancy. The noise occupancies of the modules are shown as a function of threshold-squared in Figure 7. The noise occupancies at 1 fC of the non-irradiated modules were below $1x10^{-4}$ and that of the irradiated barrel module was below $1x10^{-3}$. Those of the forward modules were one order larger than of the barrel modules which would be caused by the difference in chip temperatures.

The relation between the noise occupancy and the threshold-squared is a straight line in logarithmic scale of occupancy as the occupancy is approximated as

$$occupancy(q) \propto exp(-(1/2)(q/\sigma)^2) \quad (5)$$

where σ is the equivalent-noise-charge (ENC) of the amplifiers.

The resulting ENCs, occuENC, of the modules had little bias voltage dependence. The ENCs were obtained separately in the in-situ calibration, calibENC, with an average of ENCs at 1, 2, and 3fC, including the corrections in the section III.C. In comparison, calibENCs were systematically larger than occuENCs, which source is yet to be understood.

E. Signal-to-Noise ratios

One way of cancelling the uncertainty of the calibration capacitance is to take the ratio of the median charges to the ENCs, the signal-to-noise ratios (S/N). The S/N ratio is also an indica-

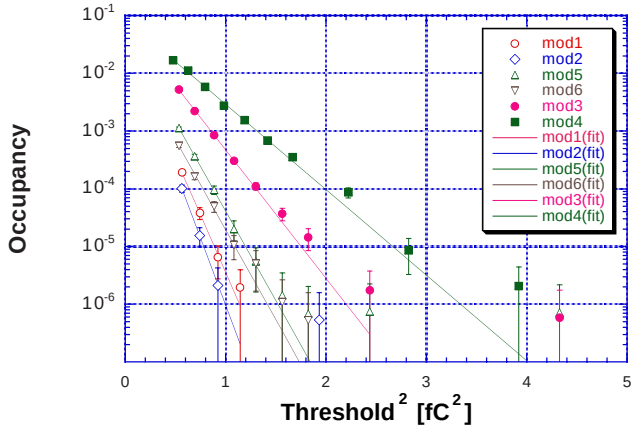

Figure 7: Noise occupancies as a function of (threshold)^2. The lines are fits to the function, exp(-1/2*(th/σ)^2)

tor of the performance where S/N > 9 would be the minimum in practical use from experience. In order to calculate the S/N, the worse ENCs, calibENC, were used for conservative reason. The resulting S/N ratios are shown as a function of bias voltage in Figure 8.

A good matching of the S/N was seen between the two barrel and two forward modules, which supported the differences of the median charges were caused by the chip-to-chip variation of the calibration capacitance. The S/N > 16 was reached above 150 V in the non-irradiated barrel, and the S/N > 10 above 300 V in the irradiated barrel modules. The S/N of forward modules were considerably lower than those of barrel modules, which would be caused by the higher chip temperatures.

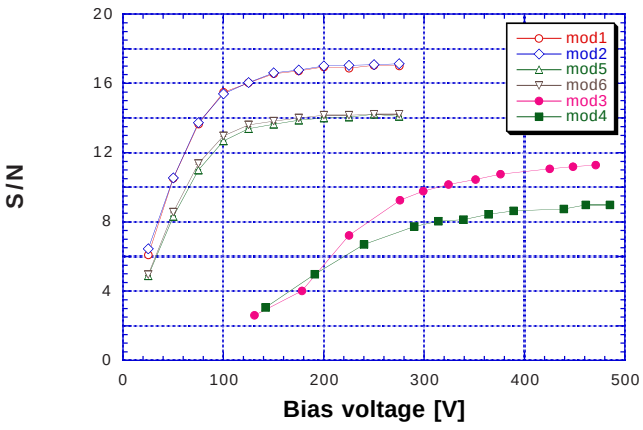

Figure 8: Signal-to-noise ratios as a function of bias voltage. The noises were averages of 1, 2, and 3 fC of the in-situ calibration

V. Summary

Two beamtests were carried out by using 4 GeV/c pions from the 12 GeV proton synchrotron at KEK for the ATLAS SCT barrel and forward modules fully equipped with the SCT specification components, including the modules irradiated to a fluence of 3x10^{14} protons/cm^2, the equivalent fluence expected in the operation of 10 years in the ATLAS detector at LHC.

The pulse shape analysis confirmed the peaking time of the amplifier to be 22 ns in the non-irradiated modules and deteriorated to 27 ns in the irradiated modules. An excess shoulder in the pulse shapes was observed which would be a feedback of the discriminator shocks. The RMS position resolutions were consistent with the uniform distribution of the pitch of 80 μm in the barrel and of 86 μm in the forward where the beam spot was. The variations of the resolutions were correlated to the fraction of the multi-hits events in the midway between the strips which gave much better resolutions.

Scanning of the threshold of the on-off readout, the median charges of the pulse height (Landau) distribution were obtained which saturated around 3.8 fC in the non-irradiated (>150 V) and irradiated (500 V) modules. The noise occupancies at 1 fC were below 1x10^{-4} in the non-irradiated and below 1x10^{-3} in the irradiated barrel modules. The ENCs obtained from the noise occupancies were systematically lower than those obtained from the in-situ calibration, which requires further investigation to understand. Using the median charges and the ENCs of in-situ calibration, the signal-to-noise ratios were >16 in the non-irradiated (>150 V) and >10 in the irradiated (>300 V) barrel modules. The matching of the S/N of the non-irradiated barrel modules indicated the spread of the median charges were caused by the variation of the chip-by-chip calibration capacitance.

The forward modules showed deterioration in two areas: (1) rise times of the pulses and larger excess shoulders, and (2) ENCs. These would be associated to much higher temperatures of the readout ASICs.

VI. Acknowledgement

The authors wish to acknowledge the cooperation of the beam channel crews of the d π2 beamline of the KEK PS and support from the ATLAS SCT collaboration.

VII. References

[1] Y. Unno et al., (1) Testbeam experiment T450, KEK, 10-20 Dec. 1999, (2) Testbeam experiment T478, KEK, 28 Nov.-10 Dec. 2000

[2] Y. Unno et al., “Evaluation of Radiation Damaged P-in-n and N-in-n Silicon Microstrip Detectors”, IEEE Trans. Nucl. Scie., Vol. 46, pp. 1957-1963, 1999

[3] DMILL technology, TEMIC Semiconductors, La Chantrerie, F-44306 Nantes, France

[4] The FR-, VAL-, and CG-modules were prepared by Univ. Freiburg, Univ. Valencia, and CERN-Univ. Geneva, respectively. The rest of the modules were by KEK

[5] W. Dabrowski, private communication